Demonstration of an ultrafast causal optical logic gate by interference of coherent transients
by Wilds David Ross

A thesis submitted in partial fulfillment of the requirements for the degree of Master of Science in Physics
Montana State University

Abstract:
An ultra fast, three port logical gate has been demonstrated using two-pulse photon echo in dye-doped polymer films at low temperatures. Since the coherence time T2 is much longer than the intervals between the excitation pulses, many more pulses can be added to the system, resulting in coherent interaction (interference) of N inputs. And finally, because of causality, pulses which come later in time do not influence the interference of those applied earlier, yet all pulses within T2 time interval interfere coherently, similar to quantum computing.

DEMONSTRATION OF AN ULTRAFAST CAUSAL OPTICAL LOGIC GATE BY INTERFERENCE OF COHERENT TRANSIENTS

by

Wilds David Ross

A thesis submitted in partial fulfillment
of the requirements for the degree

of

Master of Science

in

Physics

MONTANA STATE UNIVERSITY-BOZEMAN
Bozeman, Montana

May 1999

APPROVAL

of a thesis submitted by

Wilds David Ross

This thesis has been read by each member of the thesis committee and has been found to be satisfactory regarding content, English usage, format, citations, bibliographic style, and consistency, and is ready for submission to the College of Graduate Studies.

Dr. Aleksander Rebane — A. Rebane (Signature) — 4/9/99 Date

Approved for the Department of Physics

Dr. John Hermanson — (Signature) — 4-9-99 Date

Approved for the College of Graduate Studies

Dr. Bruce R. McLeod — Bruce R. McLeod (Signature) — 4-15-99 Date

STATEMENT OF PERMISSION TO USE

In presenting this thesis in partial fulfillment of the requirements for a master's degree at Montana State University-Bozeman, I agree that the Library shall make available to borrowers under rules of the Library.

If I have indicated my intention to copyright this thesis by including a copyright notice page, copying is allowable only for scholarly purposes, consistent with "fair use" as prescribed in the U.S. Copyright Law. Requests for permission for extended quotation from or reproduction of this thesis in whole or in parts may be granted only by the copyright holder.

Signature Nikki D Ross

Date 4-9-99

TABLE OF CONTENTS

LIST OF FIGURES

ABSTRACT

An ultra fast, three port logical gate has been demonstrated using two-pulse photon echo in dye-doped polymer films at low temperatures. Since the coherence time T_2 is much longer than the intervals between the excitation pulses, many more pulses can be added to the system, resulting in coherent interaction (interference) of N inputs. And finally, because of causality, pulses which come later in time do not influence the interference of those applied earlier, yet all pulses within T_2 time interval interfere coherently, similar to quantum computing.

Chapter 1

INTRODUCTION

In the field of optical computing, and most recently quantum computing, logic gates and switches are of great interest. A variety of non-linear optical phenomenon, including saturation of absorption, frequency conversion, Kerr effect etc, have been used in the past to implement such optical switches. Coherent optical transients in frequency selective materials provide a means of constructing analog processing devices such as correlators, delay lines and memories. Because of the non-linear nature of coherent transients, digital elements could also be produced. In this work, we present the principle of a novel, all optical logic gate based on coherent transients. We implement a three-input/three output gate, which satisfies the conditions as a universal gate, a controlled, controlled NOT. This particular type of logic gate is relevant in recent discussions about quantum computing. Although our present realization does not involve quantum mechanical entanglement of atoms, the transient photon echo phenomenon uses quantum mechanical coherence and is in this respect related to coherent and quantum computing. Such a gate is only possible because of the essential causal nature of coherent transients. To illustrate the role causality plays in coherent transient phenomenon; we present in Chapter 1, an elementary discussion of causal coherent optical response. In Chapter 2,

we present the theory and implementation of causal interference of coherent transients. We also describe the experimental setup, and the femto-second laser source. We discuss how the system behaves as an optical logic gate, and present the truth tables for both the three input/output system described here, and a four input/output system which could be constructed in a similar manner. Finally, we present a discussion of the importance of the system's causal nature to the gate's logical structure.

Chapter 2

CAUSAL COHERENT OPTICAL RESPONSE

Theory of a Linear Spectral Filter

When mathematically describing optical transient phenomenon, such as photon echoes [1] and time-and-space domain holograms [2,3], it is necessary to insure that the solution satisfies the principle of causality [4]. A causal solution is such that no response (output) appears prior to the excitation (input). If the excitation amplitude is zero for time $t<t_o$, then the response of the system must also be zero for times $t<t_o$. We set the time at which the input function begins taking effect as $t_o=0$. In complicated calculations, there is often the problem of keeping track of causality. Comparison with causal solutions found by analytic calculations can verify that, in the linear limit at least, there are only causal terms in the solution.

The causal character of coherent transients is strongly related to the nature of the system as a passive linear filter. In general terms, the frequency response of a linear system to an input has the form:

$$G(\omega) = T(\omega) F(\omega) \qquad (1)$$

Where $G(\omega)$ is the output amplitude function, $T(\omega)$ is the transmission function, and $F(\omega)$ is the input amplitude function. The filter can be described by the time-domain transmission function, or equivalently the impulse response function. Taking the inverse Fourier Transform of the above equation, we can write for the time-domain response function:

$$\begin{aligned} g(t) &= \frac{1}{2\pi}\int_{-\infty}^{\infty} T(\omega)\,F(\omega)\,e^{-i\omega t}\,d\omega \\ &= \frac{1}{2\pi}\iint T(\omega)\,f(t')\,e^{-i\omega t}\,e^{i\omega t'}\,dt'\,d\omega \\ &= \frac{1}{2\pi}\iint T(\omega)\,f(t')\,e^{i\omega(t'-t)}\,d\omega\,dt' \\ &= \int_{-\infty}^{\infty} I(t'-t)\,f(t')\,dt' = I(t)\otimes f(t) \end{aligned} \tag{2}$$

Where $g(t)$, $I(t)$, and $f(t)$ are the inverse Fourier transforms of $G(\omega)$, $T(\omega)$ and $F(\omega)$ respectively:

$$\begin{aligned} g(t) &= \frac{1}{2\pi}\int_{-\infty}^{\infty} G(\omega)\,e^{-i\omega t}\,d\omega \\ I(t) &= \frac{1}{2\pi}\int_{-\infty}^{\infty} T(\omega)\,e^{-i\omega t}\,d\omega \\ f(t) &= \frac{1}{2\pi}\int_{-\infty}^{\infty} F(\omega)\,e^{-i\omega t}\,d\omega \end{aligned} \tag{3}$$

The relation (3) is, in essence, the convolution theorem, which states that the Fourier transform of the multiplication of two functions is given by convolution of the corresponding Fourier transforms.

Now, since the time response function must be causal, the convolution integral in equation 3 must be zero for t< 0, if the temporal input function is zero for t<0. This in turn implies that the impulse response must also be zero for t<0.

$$I(t) = \begin{cases} 0, \text{ if } & t < 0 \\ I(t), \text{ if } & t > 0 \end{cases} \qquad \textbf{(4)}$$

Some mention must be made about zero time t=0. This is, of course, an arbitrary assignment of the value zero to some actual time. Time continues passing with no regard to what we label it at any given moment. We use zero here to denote the time at which a distinct event occurs. Figure 1 shows, for instance, an input amplitude function defined as starting at t=0, and ending at time $t=t_p$.

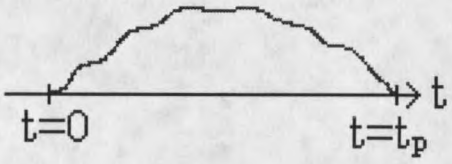

Figure 1: A temporally limited amplitude function, which is non-zero in an interval $0<t<t_p$

Titchmarch's Theorem

The practical aspect of causality is that it can often tell us something useful about the transfer function, which is helpful in performing analytic as well as numerical calculations. In particular, complex analysis provides Titchmarch's theorem [4], which describes certain mathematical properties of causal functions. This theorem relates the real and imaginary parts of a causal function to each other by means of the Hilbert transformation [6]:

$$\begin{aligned} \mathrm{Re}\,[T(\omega)] &= \frac{1}{\pi}\int_{-\infty}^{\infty}\frac{\mathrm{Im}\,[T(\omega')]}{\omega-\omega'}\,d\omega' \\ \mathrm{Im}\,[T(\omega)] &= -\frac{1}{\pi}\int_{-\infty}^{\infty}\frac{\mathrm{Re}\,[T(\omega')]}{\omega-\omega'}\,d\omega' \end{aligned} \tag{5}$$

Titchmarch's Theorem:

If a square integrable function T(ω) *fulfills one of the four conditions below, then it fulfills all four of them:*

(i) *The inverse Fourier transform* I(t) *of* T(ω) *vanishes for* t<0:

(ii) T(u) *is, for almost all u, the limit as v goes to 0+ of an analytic function* G(*u+iv*) *that is holomorphic in the upper half-plane and square integrable over any line parallel to the real axis:*

(iii) *Re* G *and Im* G *are related by the Hilbert transformation.*

(iv) *Im* G *and Re* G *are related by the inverse Hilbert transformation.*

Relation to Analytic Signal

Titchmarch's theorem is related to the analytic signal, often used in signal analysis theory. Experimentally measured time-dependent signals such as voltage, current, optical amplitude, mechanical displacement, etc. are inherently real valued functions. Their complex Fourier transforms are symmetrical with respect to $\omega=0$, and are therefore non-zero for negative frequencies $\omega<0$. In most cases however, operating with negative frequencies is not practical. Often a new complex function is defined such that the real and imaginary parts are related by the Hilbert transform, called the analytic signal [6]. The Hilbert transform of the real part is called the quadrature function. As an example, the quadrature function of $\cos \omega t$ is $-\sin \omega t$ and the corresponding analytic signal is therefore $e^{i\omega t}$. One could say that the analytic signal bears the same relationship to the real function as the complex function $e^{i\omega t}$ does to the real function $\cos \omega t$.

An optical implementation of an analytic signal can be illustrated by considering the experiment shown in figure 2. First, we place a thin cosine amplitude transmission grating of period $(\Delta\omega)^{-1}$ in the x direction, represented by:

$$T(x) = 1 + \cos(\Delta\omega x) \tag{6}$$

The grating must of course have a DC offset to prevent negative transmission values. We illuminate this grating with a monochromatic laser beam propagating in the z direction. At the output of the grating, there will be a non-diffracted transmitted beam

with a Fourier-transforming lens to produce the Fourier image of the diffracted amplitude in the back focal plane ω.

$$\hat{F}[\cos(\Delta\omega x)] = \frac{1}{2}\delta(\omega + \Delta\omega) + \frac{1}{2}\delta(\omega - \Delta\omega) \tag{7}$$

Consider now, that we place a second grating, shifted in the x direction with respect to the first grating such that it experiences a quarter period phase shift. The second grating may be represented by the function $1 + \sin(\Delta\omega x)$, next to the first grating. In addition, we will translate the sine grating by distance d along the positive z direction. The path length difference between the beam diffracted from the first and second grating is

$$\Delta x = d(1 - \cos\theta) \tag{8}$$

This will introduce a corresponding phase shift $\Delta\varphi = \frac{2\pi\Delta x}{\lambda}$. If the distance d is such that:

$$\frac{2\pi d(1 - \cos\theta)}{\lambda} = \frac{\pi}{4} \tag{9}$$

Then the total expression for the diffracted amplitude of these two gratings would be

$$\cos(\Delta\omega x)+e^{i\Delta\varphi}\sin(\Delta\omega x)=\cos(\Delta\omega x)+i\sin(\Delta\omega x)=e^{i\Delta\omega x} \qquad (10)$$

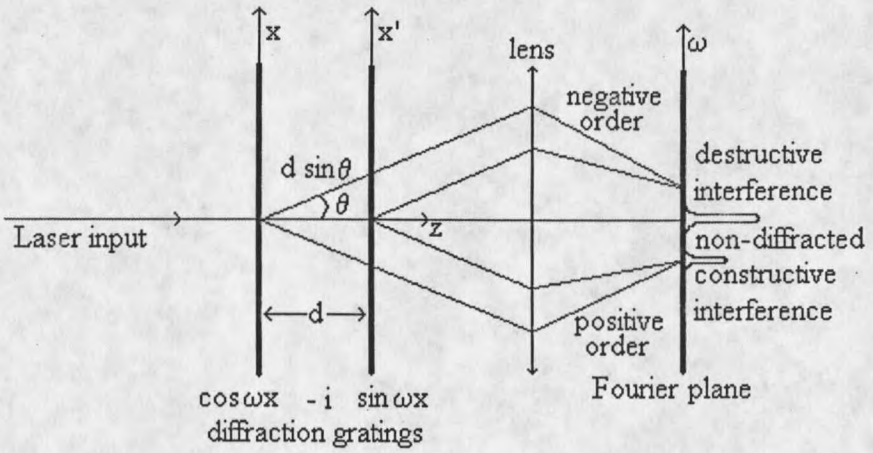

Figure 2: The optical implementation of analytic signal. x, x′-grating planes; ω-Fourier image plane

This is our "old friend" the analytic signal. The diffraction amplitude produced by the second grating combines with the amplitude of the first grating image. In the Fourier plane, the positive diffraction orders will constructively interfere, while in the negative diffraction orders they will interfere destructively. Figure 2 provides an illustration of this thought experiment. The monochromatic laser beam enters from the left to be diffracted by the cosine grating. The non-diffracted portion of the beam continues in the same direction. The beam is then diffracted by the sine grating. Again, most of this beam is not diffracted and continues along the z-axis. The diffracted beams are imaged by a lens, and allowed to interfere in the image plane. This image is the Fourier transform of the combined grating equation.

We may also consider constructing the analytic signal by simply neglecting the negative order and multiplying the amplitude of the positive order by a factor of two. Euler's formula gives for the cosine function.

$$\cos(\omega x)=\frac{e^{i\omega x}+e^{-i\omega x}}{2} \tag{11}$$

Of course, since in practice what we observe is always intensity, the constructive interference gives a four times brighter signal than that produced by one order of the cosine grating alone. This experiment has been performed in the laboratory and the results agree will with the prediction of the theory.

By virtue of Titchmarch's theorem, the Fourier image of such complex signals is identically zero for $\omega<0$. Since the experiment shown in Fig. 2 is performed with monochromatic light which extends in time from $t=-\infty$ to $t=+\infty$, causality does not really play any role here. For example, we can change the x direction phase shift from sin to – sin and then the positive diffraction order will vanish and the negative order will appear. In the case of causal time-domain transfer functions, the real and imaginary parts of $T(\omega)$ should satisfy Titchmarch's theorem, and we can rewrite $T(\omega)$ in the form:

$$T(\omega)=\mathrm{Re}\{T(\omega)\}+i\hat{H}[\mathrm{Re}\{T(\omega)\}] \tag{12}$$

Hilbert Phase

In practice, however, we can measure neither the real nor the imaginary parts of an optical response function. If electric circuits were operated at optical frequencies, then we could perhaps measure separately both the real and imaginary part of a light beam, just as we do electric signals. However, electric circuits are not capable of such an action, and in reality, we can measure only the energy (intensity) profile of a light beam. From the intensity, it is in general easy enough to find the amplitude. However, the problem remains how to find the phase. This is an issue of critical importance in many practical problems, which derive information from light measurements; i.e. astronomy, microscopy, imaging, photonics, etc. Therefore, we would like to find a way to apply Titchmarch's theorem to the complex amplitude and phase of the transmission function, rather than to the real and imaginary parts.

Corollary:

Causal transfer functions, which have Hilbert phase, can be given in the form:

$$T(\omega)=|T(\omega)|\,e^{i\hat{H}[\ln|T(\omega)|]} \tag{13}$$

Illustration:

Let

$$T(\omega) = |T(\omega)|\, e^{i\Phi(\omega)} \tag{14}$$

$$B(\omega) = \ln T(\omega) \tag{15}$$

Now consider

$$B(\omega) = \ln|T(\omega)| + i\Phi(\omega) = \mathrm{Re}\, B(\omega) + i\, \mathrm{Im}\, B(\omega) \tag{16}$$

We may identify the phase and amplitude of $T(\omega)$ *with the real and imaginary part of* $B(\omega)$. *And if* $T(\omega)$ *is sufficiently well behaved that* $B(\omega)$ *also satisfies Titchmarch's Theorem, we may write:*

$$\Phi(\omega) = \mathrm{Im}\, B(\omega) = \hat{H}[\mathrm{Re}\, B(\omega)] = \hat{H}[\ln|T(\omega)|] \tag{17}$$

$$\Rightarrow T(\omega) = |T(\omega)|\, e^{i\hat{H}[\ln|T(\omega)|]} \tag{13}$$

Spatial Holography

To better understand how the causality principle applies to time-and-space domain holography, let us first consider the coherent transmission function of ordinary thin space-domain holograms [7].

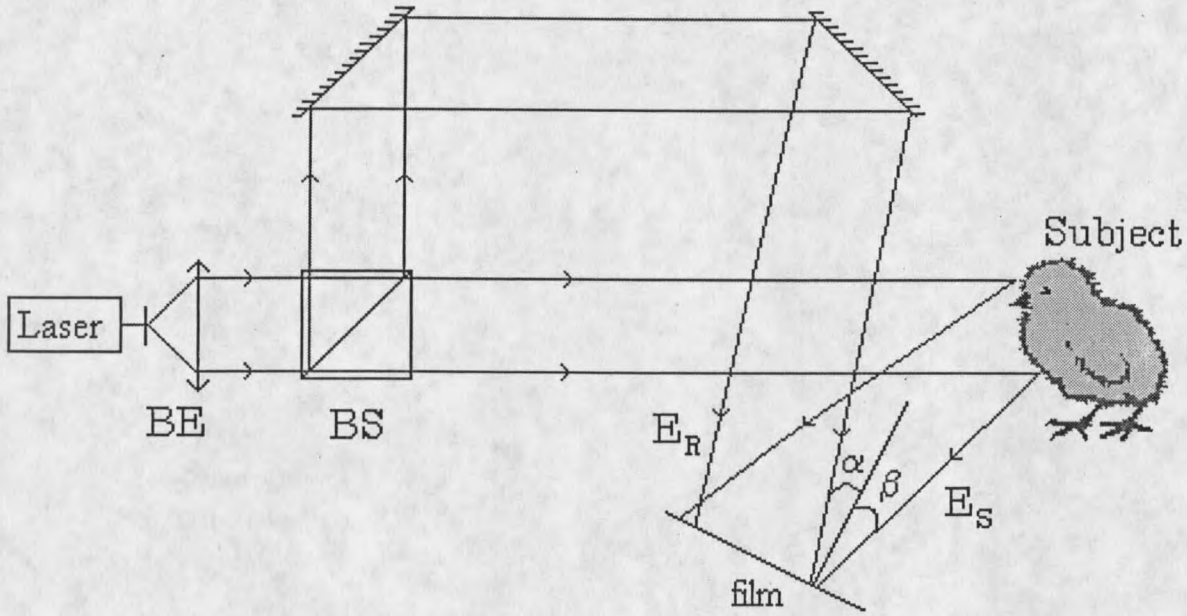

Figure 3: Scheme for recording spatial holograms: BE-beam expander; BS-50% beam splitter; E_R, E_S-amplitude of reference and subject beams.

Holography is a well-known means of recording and later recovering an optical wavefront. It does so by recording the interference pattern of two beams, which spatially overlap at the storage material, usually a photographic film. Figure 3 shows a monochromatic laser beam, which passes through a beam expander before being split 50/50 by a beam splitting cube. One of the beams remains a s a reference, while the other is scattered off the object (chicken). The two beams are then brought to coincide at a photographic film, where they form the interference pattern. The material experiences some effect e.g. a chemical reaction, which causes a change in the absorption profile of the material corresponding to the intensity profile formed by the two beams. We will construct the transfer function from the absorption properties of the material before

exposure plus the intensity dependent pattern to be "burned" into the film. Consider figure 3; the reference and subject beams are given by:

$$E_R(x,y) = r\, e^{i(\omega t+\phi)}$$
$$E_S(x,y) = s\, e^{i(\omega t+\theta)} \qquad (18)$$

Where r and s are the amplitude functions of the reference and subject beams, and ω is the laser frequency. θ and ϕ denote the phase angles containing the information on the direction of propagation of the beam relative to the normal axis of the film.

$$\phi = \frac{2\pi}{\lambda}\Delta = \left(\frac{2\pi}{\lambda}\right) x \sin\alpha \qquad (19)$$

$$\theta = \left(\frac{2\pi}{\lambda}\right) x \sin\beta \qquad (20)$$

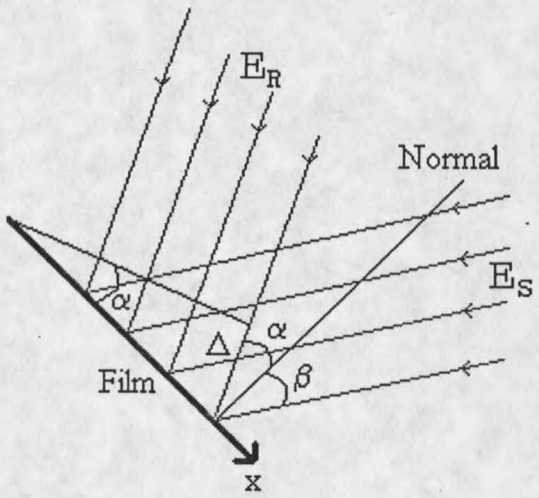

Figure 4: Close up view of the light incident on the film. The phase angles ϕ and θ are related to the spatial angles α and β through equations 14 and 15.

If we assume that the initial spatial amplitude transmission of the filter, $T_o(x,y)$ is changed by illumination in proportion to the applied intensity of light, I(x,y), then the transfer function can be written:

$$T(x,y) = T_0(x,y) + \alpha I(x,y) \tag{21}$$

Where the intensity incident on the film is:

$$\begin{aligned} I &= |E_R + E_S|^2 \\ &= |E_R|^2 + |E_S|^2 + E_R E_S^* + E_S E_R^* \\ &= r^2 + s^2 + rse^{i(\theta-\phi)} + rse^{-i(\theta-\phi)} \end{aligned} \tag{22}$$

And where the constant α includes all information about the material response properties, etc.

When a replica of the reference beam illuminates the exposed film, then the hologram acts as a linear spatial filter with a real valued amplitude transmission function (21). The amplitude at the output is given by:

$$E_H(x,y) = T(x,y)E_R(x,y) = T_0E_R + \alpha(r^2+s^2)re^{i(\omega t+\phi)} + \alpha r^2 s e^{i(\omega t+\theta)} + r^2 e^{i2\phi} s e^{i(\omega t-\theta)}$$
$$= [\text{non}-\text{diffracted terms}] + \alpha r^2 s e^{i(\omega t+\theta)} + r^2 e^{i2\phi} s e^{i(\omega t-\theta)} \quad (23)$$

In the right side of equation 23, there are two terms describing the diffraction process. One of the terms has the same phase, and amplitude as the subject beam, it propagates in the same direction as the subject beam and represents a virtual image of the subject. This term represents the first positive diffraction order. The second term is phase conjugated with respect to the subject beam, and is propagating at a different angle. This beam is the first negative diffraction order. An illustration of the diffraction process is shown in figure 5. Note that there are no restrictions on the direction of propagation of the diffracted beams about the read-out beam, and both positive and negative diffraction orders can be produced simultaneously.

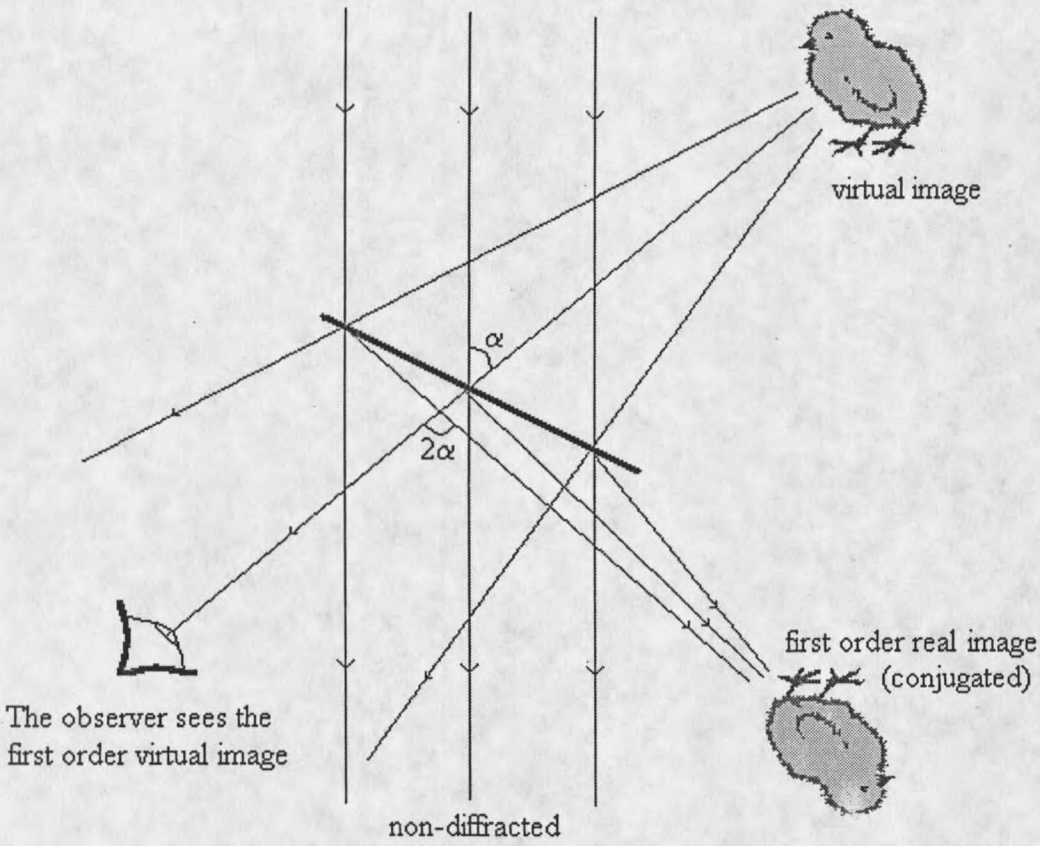

Figure 5: Reconstruction of image by a thin transmission hologram.

Spectral Hole Burning

Recording and readout of spectral hole burning holograms is similar to the procedure described above, with the difference that SBH holograms make use of frequency selective materials. The absorption of SHB materials may be saturated at a given frequency, and a "spectral hole" may be formed. Any subsequent incident beams will then be modified by the material's new absorption profile. In these materials, the amplitude frequency response to a particular frequency is essentially independent from

the response at other frequencies. SHB is based on the fact that certain atoms or molecules may experience a chemical or a physical change in which the product of this reaction has an absorption distinct in frequency from the educt. This is a very powerful tool for it allows virtually any custom pattern to be "burned" into the transmission spectrum of the material.

Of critical importance to SHB is the existence of a zero phonon line. ZPL is essentially a resonance absorption line in an atom or molecule embedded in a solid matrix such as a crystal, glass, polymer etc. The ZPL contains no coupling with phonons, which becomes possible at liquid helium temperatures. The ZPL can have a very narrow homogeneous line width Γ_{hom}. Since no molecule experiences exactly the same local environment as the others, the measured absorption profile is considerably broader than the ZPL width. This effect is called inhomogeneous line broadening, and is characterized by the width of the inhomogeneous distribution function Γ_{inh}. Figure 6 shows how the inhomogeneous line is the sum of the individual absorptions from each homogeneous line, which are frequency shifted relative to each other by the random nature of the environment. The term Spectral Hole Burning refers to the process of saturating the absorption of a single homogeneous line, producing a dip, or hole in the inhomogeneous distribution. The capacity for storing information is given by the ratio of the Γ_{inh} to the Γ_{hom}. For the purpose of holography it is, of course, favorable to have as good resolution as possible and therefore a broad Γ_{inh} and narrow Γ_{hom}.

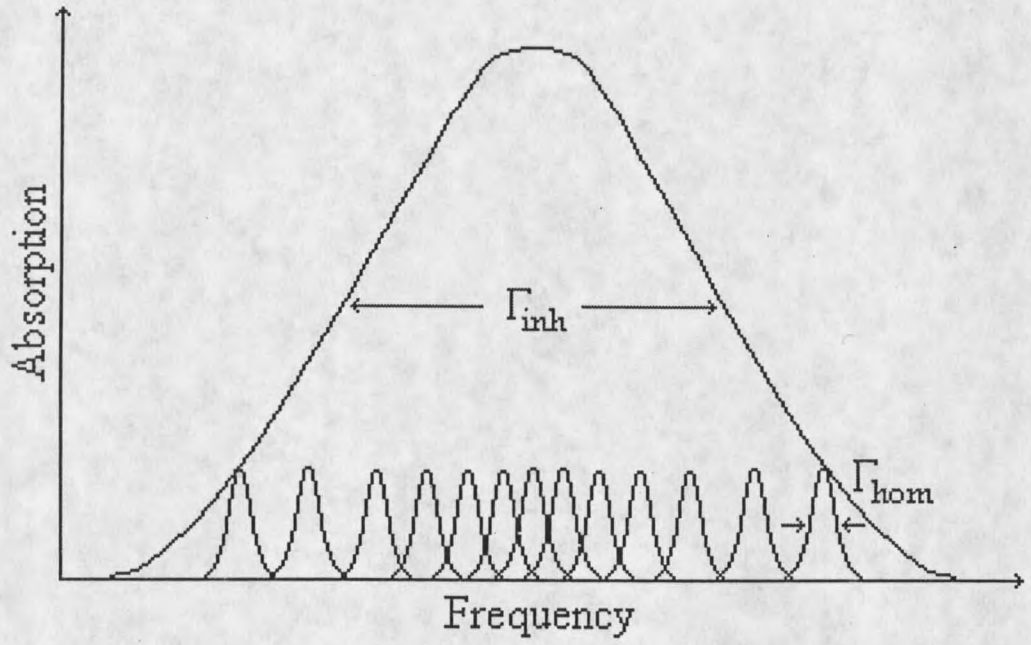

Figure 6: An inhomogeneously broadened absorption line. The distribution of local environments leads to a distribution of center frequencies for absorption.

Time-and-Space Domain Holography

Time domain holography is an example holographic readout of SHB materials. The time bandwidth product requires that if the beam is to consist of short pulses in time, on the order of τ_p then it has to have a broad spectrum on the order of $1/\tau_p$. These pulses are then allowed to interfere with each other in the SHB material. The writing pulses may be separated from each other in time, provided the material does not "forget" the phase information of the first pulse, before the second pulse arrives. The limiting factor in this case is the dephasing time, which is the Fourier dual of the homogeneous line width. The difference in arrival time between the reference and subject pulses is

expressed mathematically as a phase shift. The separation between pulses is typically large compared to the pulse duration as shown in figure 7.

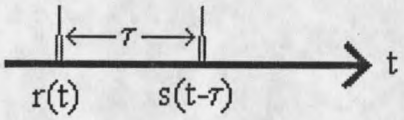

Figure 7: The writing pulses in the time domain

SHB materials are sensitive to spectral intensity as well as spatial intensity. In order to describe the amplitude transmission of SHB holograms both the spatial as well as the optical frequency coordinates must be included. The interference of the two pulses produces an intensity pattern in frequency and in space, which is stored in the absorption profile of the material. During the read out, the material acts as a linear filter, transmitting certain frequency components more than others. It also is introducing a phase shift between different spectral components. The linear, frequency domain response of the SHB medium is described by (1). Because the impulse response I(t) is in this case necessarily a causal function, the real and imaginary part of $T(\omega)$ must be related according to (5). On the other hand, spectral intensity transmission is a real function, whose imaginary part is zero. Therefore, we may surmise that a simple real-valued transmission of SHB media cannot satisfy the causality requirement.

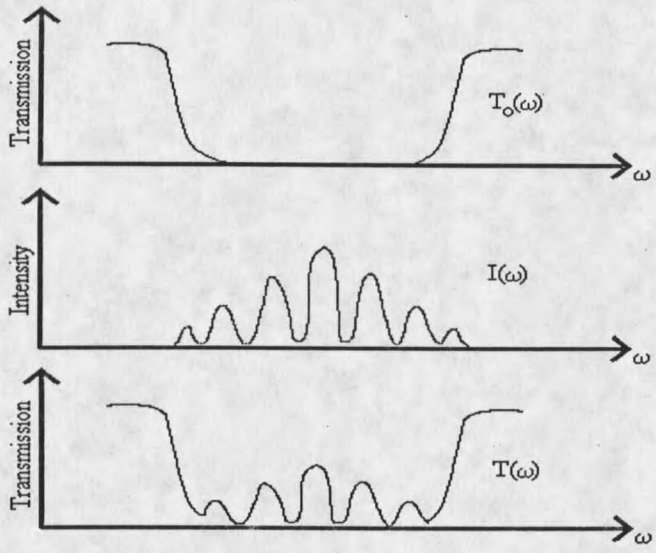

Figure 8: The frequency domain transmission function

To illustrate this point, let us first assume that, in full analogy to the spatial hologram, the transmission function is changed in proportion to the illuminating intensity. The transmission function will be taken, as illustrated in figure 8, the sum of $T_o(\omega)$, the transmission before exposure, and $\alpha I(\omega)$ the scaled intensity incident on the film:

$$T(\omega) = T_0(\omega) + \alpha I(\omega) \tag{24}$$

The reference and subject beams arrive separated in time by t, and form an interference pattern $I(\omega)$.

$$\begin{aligned} I(\omega) &= \left|\hat{F}[r(t)] + \hat{F}[s(t-\tau)]\right|^2 \\ &= \left|\hat{F}[r(t)] + e^{i\omega t}\hat{F}[s(t)]\right|^2 \\ &= \left|R(\omega) + e^{i\omega t}S(\omega)\right|^2 \end{aligned} \tag{25}$$

The transmission function is now given by:

$$\begin{aligned} T(\omega) &= T_0(\omega) + \alpha\left(|R(\omega)|^2 + |S(\omega)|^2 + R^*(\omega)S(\omega)e^{i\omega t} + R(\omega)S^*(\omega)e^{-i\omega t}\right) \\ &= [\text{non} - \text{diffracting terms}] + \alpha R^*(\omega)S(\omega)e^{i\omega t} + \alpha R(\omega)S^*(\omega)e^{-i\omega t} \end{aligned} \tag{26}$$

When a replica of the reference pulse is used to illuminate the medium, the time response is expressed as:

$$g(t) = \frac{1}{2\pi}\int_{-\infty}^{\infty} T(\omega)R(\omega)e^{-i\omega t}d\omega \tag{27}$$

$$\begin{aligned} g(t) = [\text{non} - \text{diffracted terms}] \\ + \frac{\alpha}{2\pi}\int_{-\infty}^{\infty} e^{i\omega t}\hat{F}[r(t')]\hat{F}[r(t'')]^*\hat{F}[s(t''')]e^{i\omega\tau}d\omega \\ + \frac{\alpha}{2\pi}\int_{-\infty}^{\infty} e^{i\omega t}\hat{F}[r(t')]\hat{F}[r(t'')]\hat{F}[s(t''')]^*e^{-i\omega\tau}d\omega \end{aligned} \tag{28}$$

Let us simplify equation 28 by expressing the Fourier transforms as integrals, and by regrouping the exponential terms. We may identify the Dirac delta function in the first diffracted term:

$$\frac{\alpha}{2\pi}\int_{-\infty}^{\infty} d\omega \iiint_{\infty} dt' dt'' dt''' r(t') r^*(t'') s(t''') e^{i\omega(-t+t'+t''+\tau)} \tag{29}$$

By definition,

$$\int_{-\infty}^{\infty} e^{i\omega(-t+t'+t''+\tau)} d\omega = \delta(t''' - (t - t' + t'' - \tau))2\pi \tag{30}$$

The integral (28) then reduces to:

$$\begin{aligned} &\alpha \iiint_{\infty} dt' dt'' dt''' \, r(t') r^*(t'') s(t''') \delta(t''' - (t - t' + t'' - \tau)) \\ &= \alpha \iint_{\infty} dt' dt'' \, r(t') r^*(t'') s(t - t' + t'' - \tau) \end{aligned} \tag{31}$$

If we set,

$$r(t') = \delta(t') \tag{32}$$

Then (28) further reduces to:

$$\alpha s(t + \tau) \tag{33}$$

This term represents the image of the subject pulse. It corresponds to the first positive diffraction order. It is emitted at a time after the read pulse equal to the time between the first two pulses.

Similarly, we obtain for the other term:

$$\frac{\alpha}{2\pi}\int d\omega\iiint dt'dt''dt''' \, r(t')r(t'')s^*(t''')e^{i\omega(-t+t'+t''-t'''-\tau)} \\ = \alpha s^*(-(t+\tau)) \tag{34}$$

This term represents the first negative diffraction order. However, it appears to be emitted at a time before the read pulse. This term is not causal, and is therefore not physically meaningful. The other feature of this term is that the image goes backward in time, which is an analog of phase conjugation in the space domain. The non-causal time domain response function is shown in figure 9.

Since the temporal response we have obtained is not causal, then there must be something wrong with the way we have calculated the transmission function (24). The entire solution is incorrect, and a new solution must be found by constructing a complex function T(ω).

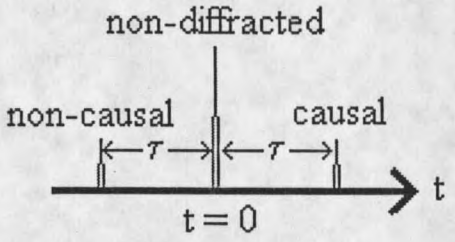

Figure 9: The non-causal time domain response function

Constructing a Causal Response Function.

First, let us note that the transmission (24) gives amplitude transmission only, while the frequency dependent phase is not present. We may try to construct the missing phase using the modified Hilbert relationship.

$$T(\omega) = |T(\omega)| \, e^{i\hat{H}[\ln|T(\omega)|]} \tag{35}$$

Some computer software does not provide the Hilbert transform but do provide the Fast Fourier Transform. When calculating the Hilbert transform numerically, it is desirable to use the Fast Fourier Transform exclusively. On the computer, specifically in the program Mathematica, the input, output, and transfer functions are just lists of numbers. Therefore, we may make use of the causal properties of the Hilbert transform in the impulse response in a more basic way. To obtain the Hilbert transform we take the Fourier transform of the logarithm of the amplitude transfer function. Then we delete the portions of the list corresponding to negative argument values. Then take the inverse Fourier transform to find the Hilbert phase of the causal transmission function.

The results of such a calculation are given below. Figure 10 is a plot showing the two excitation pulses. Note that the write pulse and the subject pulse are identical and delayed by time t.

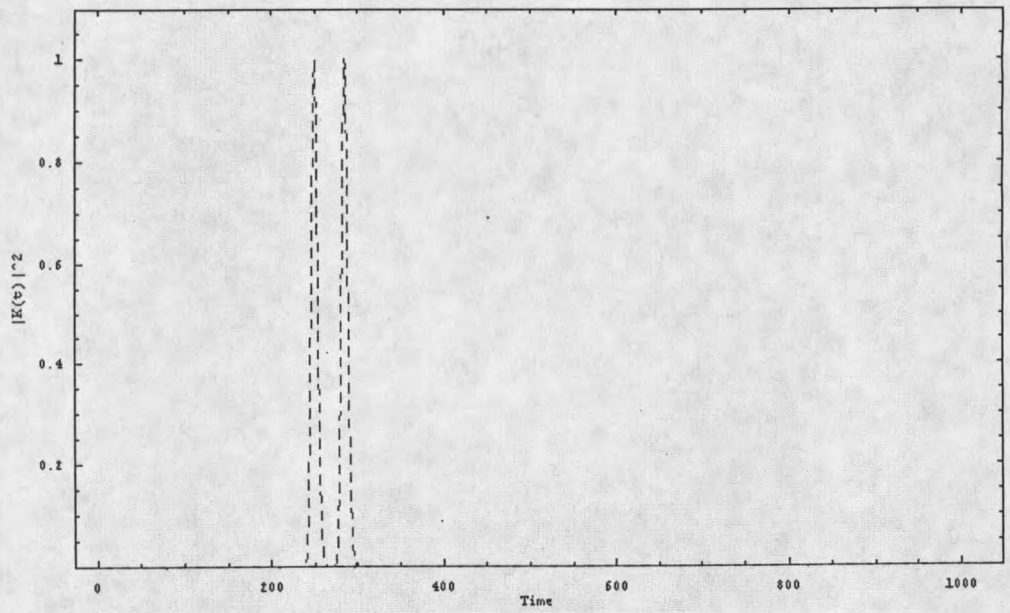

Figure 10: Write and subject pulses

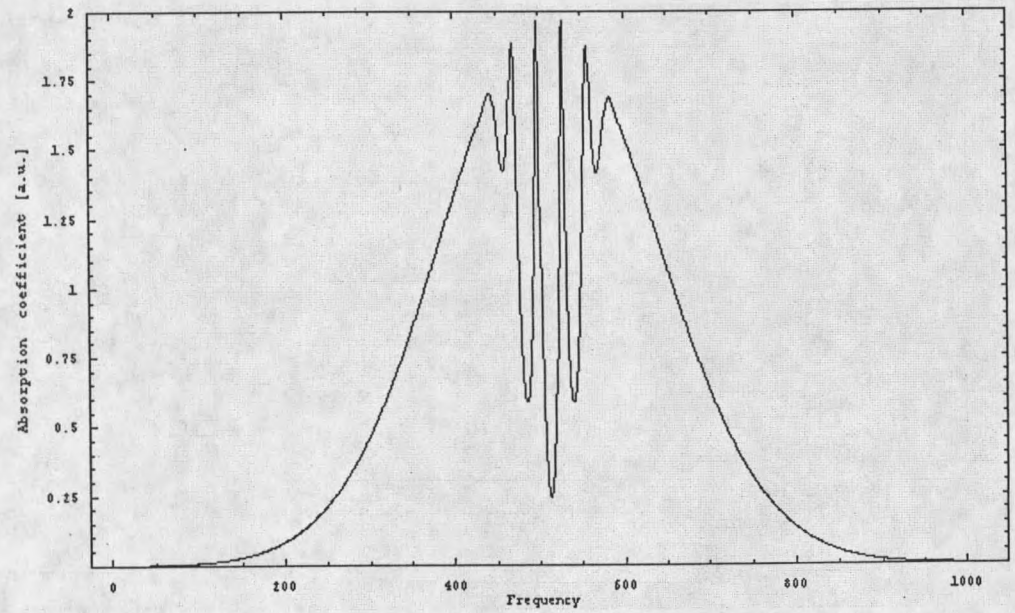

Figure 11: The burned-in interference pattern formed by the pulses in figure 10 These two pulses' spectra interfere in the SHB medium to form an interference grating, figure 1, whose period is 1/t.

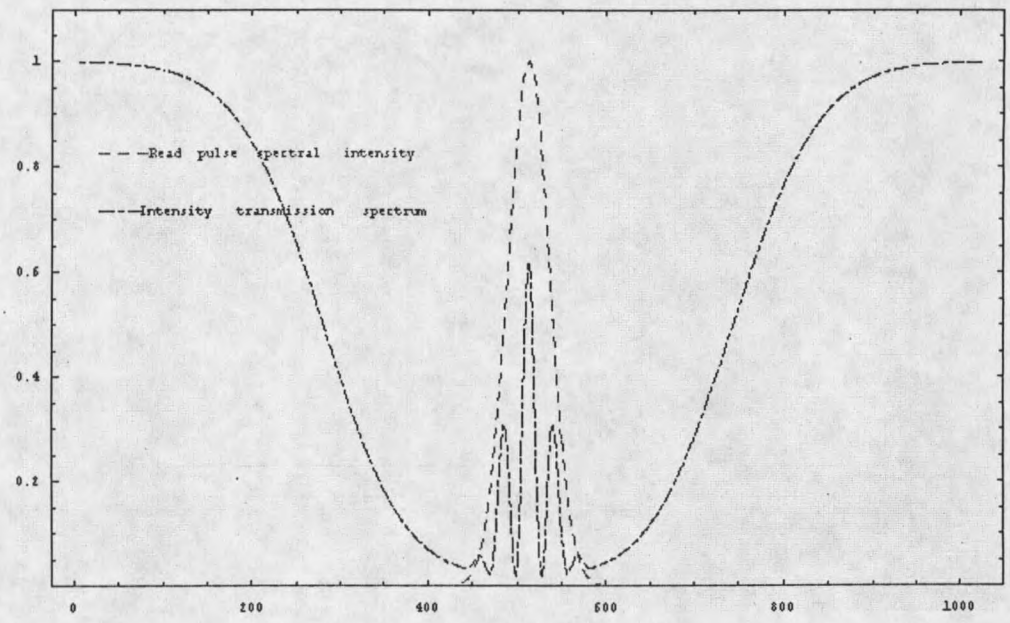

Figure 12: The amplitude transmission function

The amplitude transmission function is shown in figure 12. It is the sum of the background absorption spectrum and the intensity grating in figure 11. It is an expression of equation 24. Superimposed over this image is the read pulse spectrum. The read pulse is again identical to the excitation pulses in figure 10.

The response function is shown in figure 13 (a). Both the non-causal solution, found from the amplitude transmission function, and the causal solution, found from the Hilbert phase transmission function are displayed. The non-causal response function has an image of the subject pulse appearing prior to the read out pulse. One might be tempted to just throw that part of the response function away.

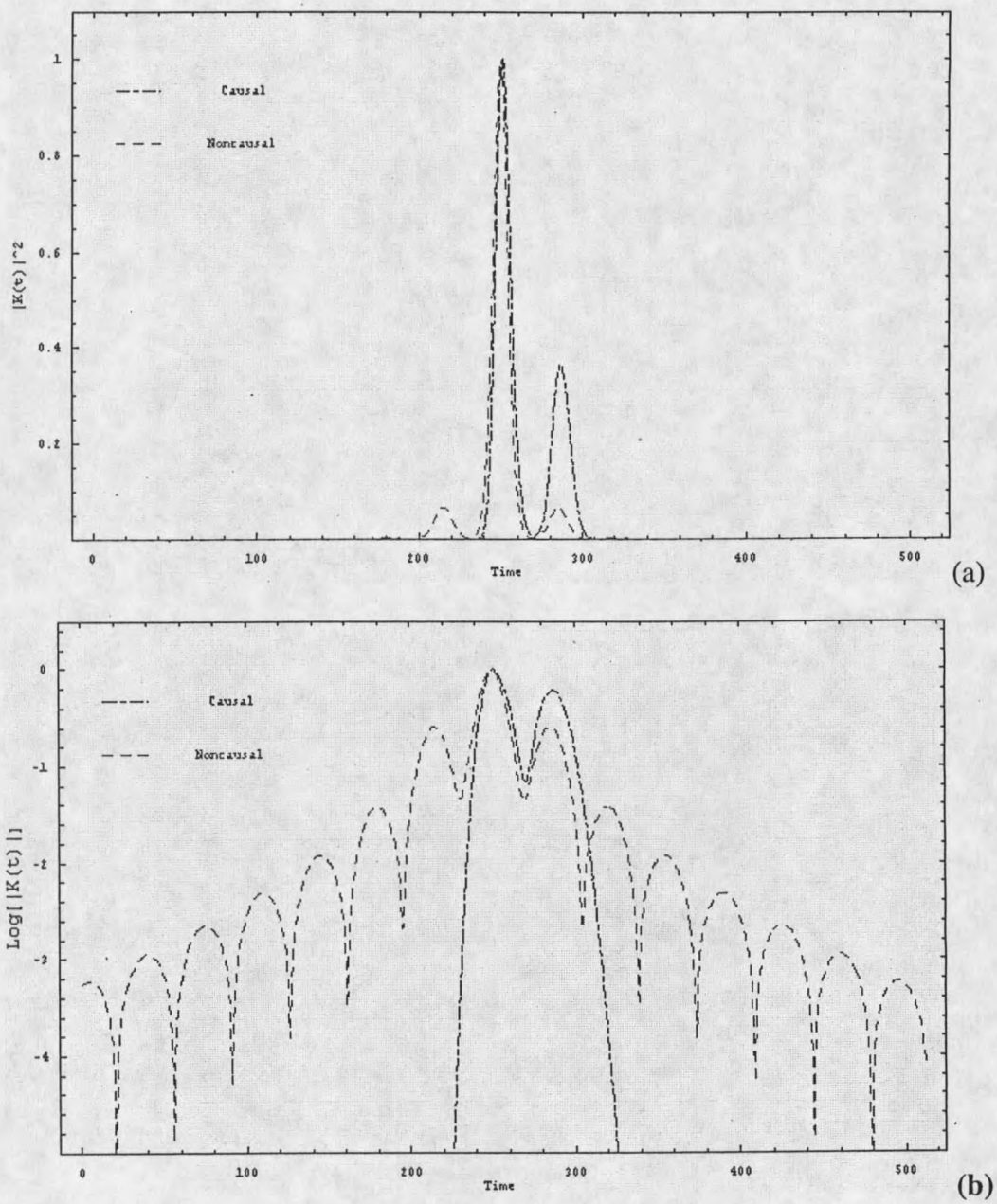

Figure 13: The causal and non-causal response functions. (a) linear plot (b) log plot of the same functions

However, figure 13(b) is a log plot of figure 13(a), and as you can see, there are many artifacts in the non-causal solution, such as additional pulses also appearing in the allowed temporal direction. It is not immediately evident that these are not causal terms.

Indeed, in a general calculation it is often unclear which elements should be eliminated. However, there is at least one way to ensure that all the terms in the solution are causal, and that is to construct the transmission function with Hilbert phase.

Another conclusion immediately obvious from the figures above, is that the causal solution has higher intensity than the positive order non-causal solution. This corresponds to a doubling of the amplitude as discussed in section 1.3, concerning the analytic signal.

Non-linear calculations, such as numerical integration of the optical Bloch equations, must also give causal response functions. Through investigations into the linear response it is evident that modifying the transmission function to have Hilbert Phase is the appropriate adjustment to ensure causality it obeyed.

Chapter 3

CAUSAL OPTICAL LOGIC GATE

In this chapter, we would like to illustrate an application of the causal nature of coherent optical transients. Due to the current interest in quantum computers and optical computing elements, it may be interesting to consider a digital optical logic gate, which makes use of these properties.

Interference of Coherent Transients

It is a requirement of quantum gate arrays that they must be reversible [5]. That is, knowing the quantum state of the output channels tells uniquely what is the quantum state of the input channels. This is a result of the fact that the laws of physics are completely reversible in time. There exist two universal gates for reversible computations, the Taffoli gate and the Fredkin gate. These gates are universal in the same sense that a NAND gate is universal for classical computations. Since classical computations are not reversible, any classical computation can be performed with an array of NAND gates. Similarly, any quantum, and therefore reversible, computation can be performed with an array of Taffoli or Fredkin gates. We will attempt to show that by means of coherent optical transients it is possible to construct a Taffoli gate. However, for this to be the case, there must be no back effect from pulses applied later in time on

pulses applied earlier. This is precisely the causality condition described in Chapter 1. Therefore, the logic gate described here is a causal Taffoli gate, and has the arrow of time built in.

Our idea is to generate a two-pulse photon echo, angularly resolved from the input pulses. Then send into the medium a third pulse in the same direction as the echo signal. The third pulse can then interact with the echo, and possibly produce interference. In this way, we have made a system with three inputs and three outputs. The logic element function, which we want to achieve, is called "controlled, controlled NOT." This means that the first two pulses act as two controllers of the NOT operation: the third pulse only occurs if both the first two pulses are present. To achieve this, the first two pulses generate a photon echo, and if the third pulse is allowed into the system, then the echo and the third pulse interfere destructively. Ideally, a detector measuring the energy of the third pulse at the output of the sample will detect zero intensity. If the third pulse is not allowed to pass through the medium, then the echo pulse appears at the detector, and the intensity is not zero. The truth table corresponding to this logic gate is given by figure 23, and will be discussed in detail below.

We need to confront a practical problem as well. The ideal destructive interference between the echo and the third pulse is only possible if the temporal and spatial wave fronts exactly overlap. In practice, however both the echo and third beam are always somewhat distorted by the optics used in the experiment. Our experiment reveals to what extent this problem can be resolved.

Experimental

Figure 14 shows the constituent parts of a regenerative amplified femtosecond laser system. An Argon ion laser (Coherent Inova 400) pumps a Ti: Sapphire oscillator (Coherent Mira 900). The ion laser produces ~8 W/cm^2 of visible multiline power, and is fitted with the Coherent PowerTrack system, a pair of piezoelectric transducers on the end mirrors, to stabilize the output power. The pulsed mode can be viewed as a Fourier sum of continuous wave modes in the cavity that are phase locked to each of the different frequencies. The pulsed mode is produced by constructive interference of the different frequencies at the time of the pulse, and destructive interference at the times between the pulses. The high intensity produced by the short pulses results in Kerr lensing in the Ti:Sapphire crystal. The lensing effects reduce the cross sectional area of the pulse mode, while the relatively low intensities of the CW mode results in very little intensity dependence on the beam diameter. The pulsed mode is then "selected" in the cavity through the introduction of a spatial filter, an adjustable slit, which allows the smaller diameter pulsed mode to pass through. However, the slit clips the edges of the CW mode and prevents this mode from lasing. Since the CW mode does not achieve the intensity necessary to begin Kerr lensing in the crystal, some other mechanism must be introduced in the cavity to begin the modelocking process. This is achieved with a small glass plate, which vibrates rapidly changing the angle, through the glass, which the beam passes. This changes the path length of the beam in the cavity and increases the number of modes oscillating. When a sufficient number of modes are active, the peak intensity will go up

to the point that Kerr lensing begins taking place in the crystal, and these modes are then spatially selected as mentioned above. Once the modelocking process has begun, the glass plate may come to rest, as there is no further need for the starting mechanism. In this way, the oscillator generates pulses on the order of hundreds of femtoseconds at 76 MHz. The time-bandwidth product insures that these pulses will have a broad range of frequencies, ~5-6 nm FWHM, which is desirable for SHB holography experiments. The central wavelength of the Mira 900 is tunable between 700-1000nm. The time averaged power, while somewhat dependent on wavelength is ~800 mW, with a beam size of ~1 mm^2.

In the regeneratively amplified system, these pulses pass through a Faraday isolator, as the oscillator is quite sensitive to feedback. The pulses must be stretched before entering a Ti: Sapphire regenerative amplifier to avoid damage to the amplifier crystal. The stretcher is simply a multipass diffraction grating, and the output is on the order of 100 pico-seconds. These pulses seed a Ti:Sapphire regenerative amplifier (Clark TRA-1000). A Q-switched YAG (Clark ORC-1000) lasing at 532 nm and 1KHz pumps the amplifier at 8 W/cm^2. The timing is somewhat delicate and is controlled by a pockels cell. The amplifier amplifies all frequency components and may saturate at the frequencies with the highest intensity, therefore the spectrum of the pulses coming out of the amplifier is somewhat broader ~8-10 nm FWHM than those coming out of the oscillator. The time-averaged power in the amplified pulses is close to 1 watt. The output of the amplifier must again pass through the optical isolator along the same path as the pulses came in, and they are then compressed back to hundreds of femtoseconds.

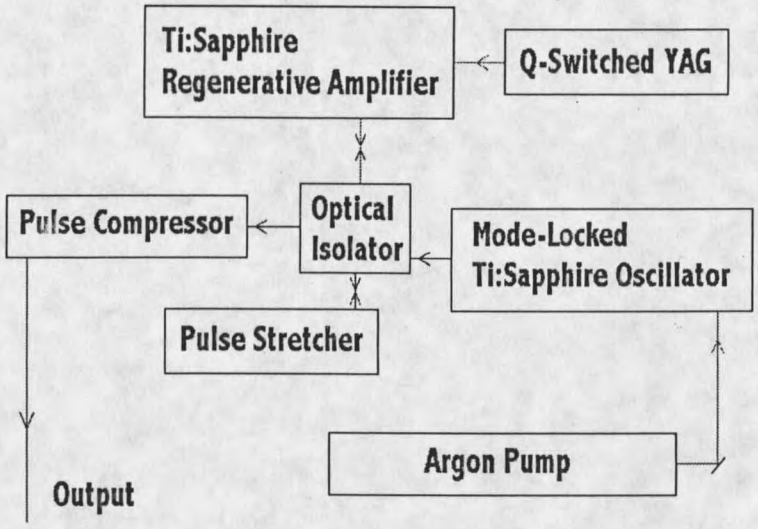

Figure 14: The laser system

Following compression, the pulses have the following parameters: time averaged power ~1 W/cm^2, spectral width ~8-10 nm, temporal duration ~150 fs, spatial profile ~1 cm^2. The experiment setup is shown in figure 15. The output pulses from the laser system enter the top of the figure and pass through a beam expander and pinhole (not shown) in order to make the spatial profile as even as possible. Next, the beam passes through a beam splitter, which selects approximately 50% of the power. The beam which is reflected to the right then passes through a thin piece of glass to select a small component of the beam ~2% (only one of the two reflections are used). The remaining portion of the beam then passes through a prism to reflect the beam back to the direction of the sample chamber of the cryostat. This is beam 1. Beam 2 emerges from the beamsplitter cube, then reflected by a pair of mirrors on a translation stage up to a mirror

that will reflect the beam into the sample chamber. The small angular difference relative to the first beam is $\theta \sim 1°$.

The translation stage allows for the delay τ_{21} to be adjusted for maximum echo signal. The third beam came off of the glass slide which is also mounted on a separate translation stage, to allow the third beam delay τ_{31} to be adjusted, and then is reflected by a pair of mirrors into the sample chamber. All three beams spatially overlap in the sample and emerge on the other side again angularly resolved from each other. The three beams are then captured with a video camera.

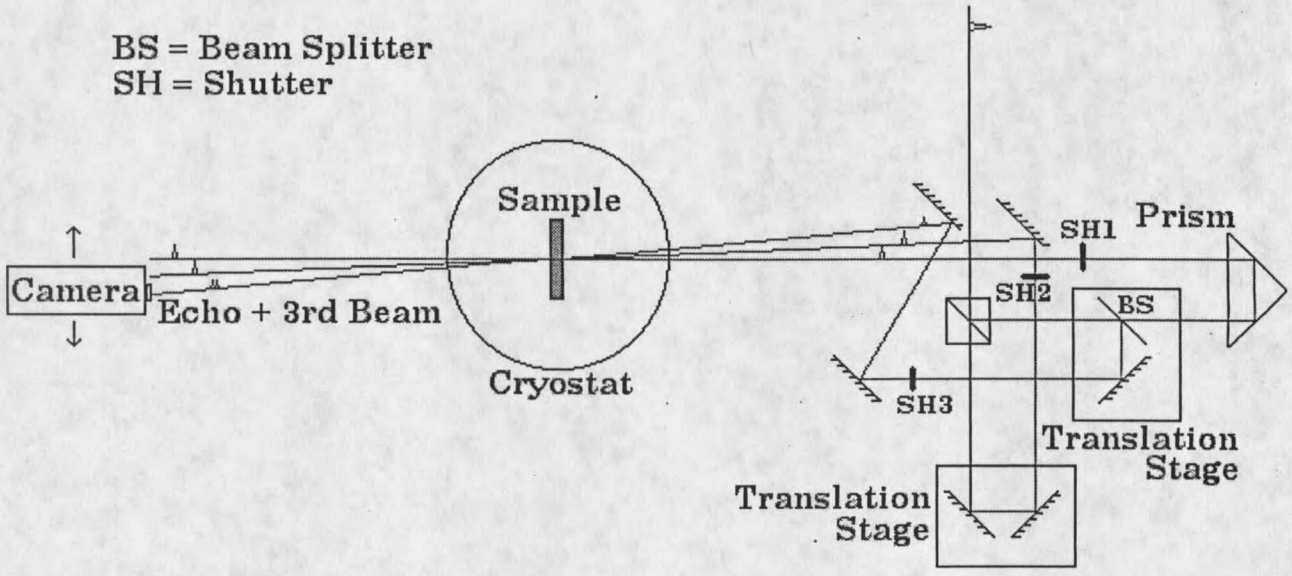

Figure 15: Experimental Setup

The SHB sample consists of a PVB film doped with Naphtalocyanine type (Ciba 1009) molecules. The PVB is dissolved in methanol and the dye molecules are added to the solution. The solution is then poured on a glass plate and the methanol allowed to evaporate. The resulting film can then be peeled off the glass plate. Since the optical

quality if rarely good at this point, the film is pressed between glass slides while being heated at 100° – 150° F. The thickness of the sample can be regulated during this stage. The absorption spectrum of the sample is shown in figure 16. The spectral hole burning takes place in the right most absorption peak. This transition is from the ground state singlet S_o to the first excited singlet state S_1. Γ_{inh} for this transition is quite broad due to the random environment of the polymer film ~10 Terahertz at 2°K. While at this temperature Γ_{hom} is ~360 MHz.

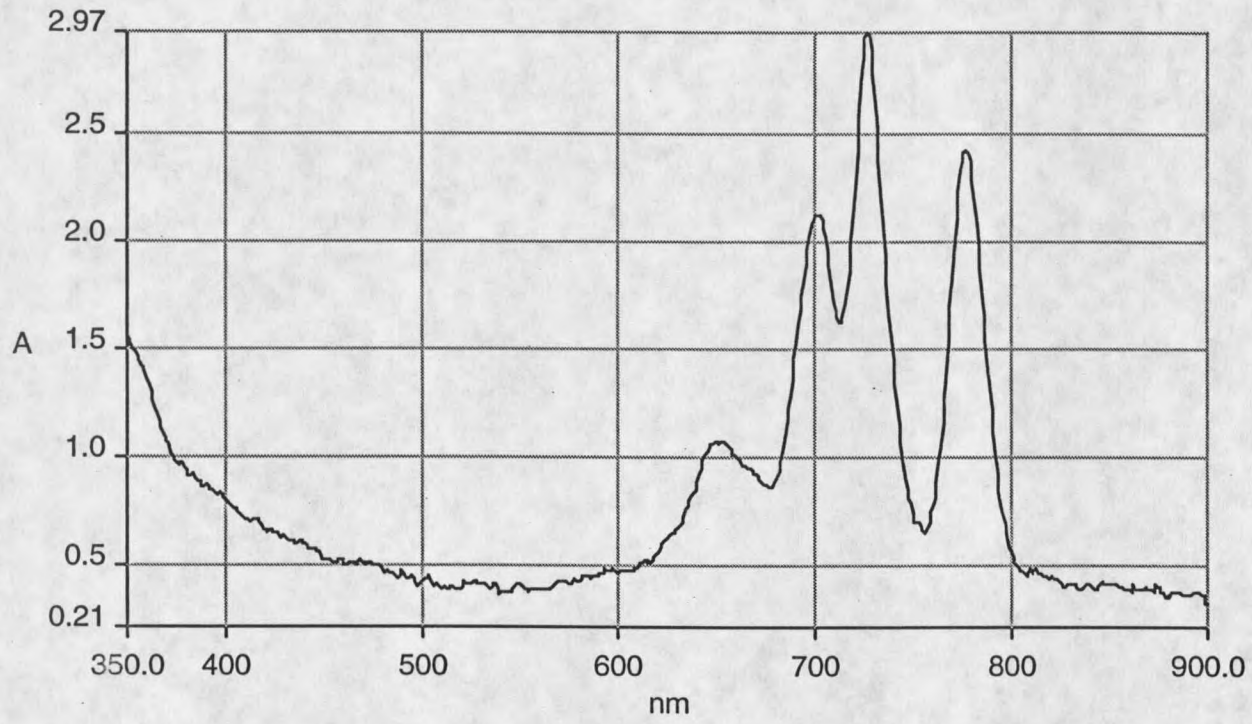

Figure 16: Absorption Spectrum of the Sample

Generation of an Off Axis Two Pulse Photon Echo

The off axis two pulse photon echo is generated by directing two short laser pulses such that they spatially overlap at the SHB medium. The spot size of each pulse is ~1 cm^2, and the time-averaged power in the excitation pulses has been attenuated to the order of 5 mW/cm^2. The amplitude of a single excitation pulse in each direction is given by:

$$E_1(\vec{r},t) = \varepsilon_1(t-\eta_1)e^{i\omega(t-\eta_1)}$$
$$E_2(\vec{r},t) = \varepsilon_2(t-\eta_2)e^{i\omega(t-\eta_2)} \quad (36)$$

Where the parameter $\eta_i = \frac{\vec{k}\cdot\vec{r}}{c} + t_i$.

The pulses need not overlap in time, but the delay between the arrival of the pulses τ_{21} must be less than the optical coherence time of the material T_2~0.5 ns. The echo is emitted a time after the second pulse, equal to the time between the arrival of the first two pulses, $\tau_{21} = \tau_{e2}$. The echo amplitude is given by:

$$E_e(\vec{r},t) = \varepsilon_e(t-\eta_e)e^{i\omega(t-\eta_e)} \quad (37)$$

Where

$$\eta_e \equiv 2\eta_2 - \eta_1 \tag{38}$$

is the phase matching condition. This implies that the interaction length for the excitation pulses is long enough to completely cover the sample width so that the contributions to the echo signal from successive slices of the medium are in phase and add together coherently. This insures that there is maximum efficiency in the echo generation process. If the two input beams are set at some spatial angle θ relative to each other, then the echo signal will be emitted from the medium at the same angle θ relative to the second pulse. Figure 17 shows the geometry of the generation of the echo. The pulses shown are meant to portray the temporal spacing of the pulses. As such the figure represents two temporal "snapshots" of the system, before arrival of the pulses at the sample, and after the pulses leave the sample.

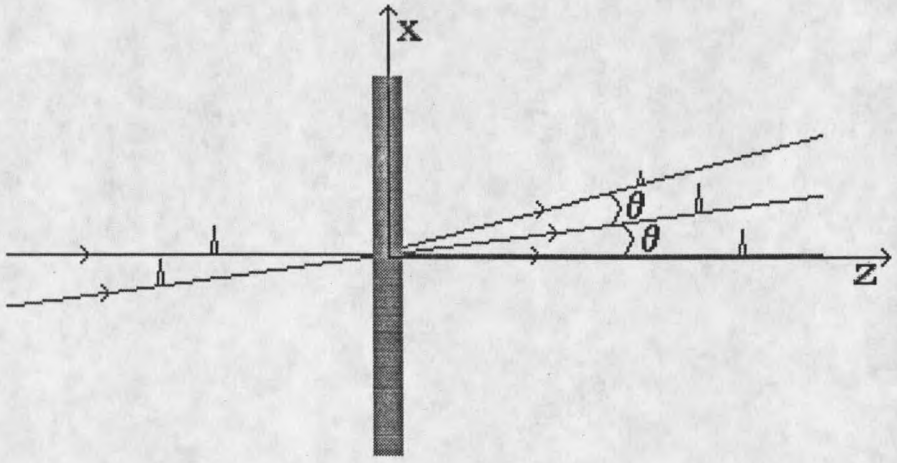

Figure 17: Generation of Off-Axis Two Pulse Photon Echo

Let us consider now that a third beam is introduced such that it propagates in the same direction, and with the same delay, as the echo signal, such as in figure 18. A detector positioned at the output of the signal will record intensity:

$$I = |E_3 + E_e| = |\varepsilon_3|^2 + |\varepsilon_e|^2 + \left(\varepsilon_3 \varepsilon_e^* e^{i\omega(\eta_3 - \eta_e)} + c.c.\right) \tag{39}$$

Where E_3 is:

$$E_3(\vec{r}, t) = \varepsilon_3(t - \eta_3) e^{i\omega(t - \eta_3)} \tag{40}$$

Let us assume that $\vec{k}_3 = \vec{k}_e$, and $\varepsilon_3 = \varepsilon_e$, which means that the intensity will be:

$$I = 2|\varepsilon|^2 + |\varepsilon|^2 \left(e^{i\omega(t_e - t_3)} + e^{-i\omega(t_e - t_3)}\right) = 2|\varepsilon|^2 \left(1 + \cos\omega(t_e - t_3)\right) \tag{41}$$

This expression describes interference between the photon echo and the third pulse. For destructive temporal interference:

$$t_e - t_3 = \frac{(2n+1)\pi}{\omega} \quad \Rightarrow \quad \text{Delay} = c(t_e - t_3) = n\frac{\lambda}{2} \tag{42}$$

And for constructive interference:

$$t_e - t_3 = \frac{2n\pi}{\omega} \quad \Rightarrow \quad \text{Delay} = c(t_e - t_3) = n\lambda \tag{43}$$

This means that, for destructive interference, the total delay of the third pulse relative to the first pulse is equal to $\tau_{31}=2\tau_{21}+n\lambda/2c$.

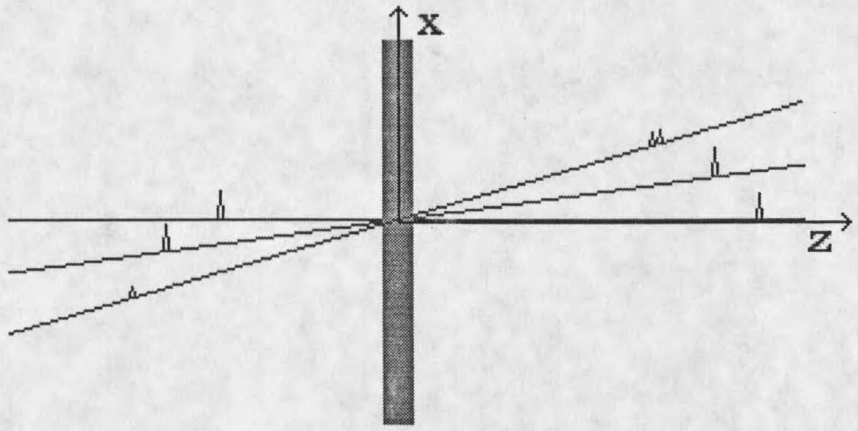

Figure 18: When a third pulse is introduced colinearly with the photon echo, interference may be observed

Results and Discussion

We will show now that such a three-beam arrangement can be operated as a logic gate. Consider the system as having three inputs and three outputs, where the output depends in a nonlinear manner on the input. The first non-linearity occurs in the generation of the 2PPE: The echo pulse is present if and only if both of the first two

excitation pulses are applied. If either of the first two inputs are zero, then the echo is not produced. Also, if the third pulse is present, then destructive interference will take place between the third pulse and the echo signal excited by the first two pulses.

The photon echo as imaged at the camera and its intensity profile can be seen in figure 19. The image was captured by inserting SH3 in figure 15. The horizontal line in the picture shows the axis from which the intensity profile was taken. The intensity of the pulse is in arbitrary units.

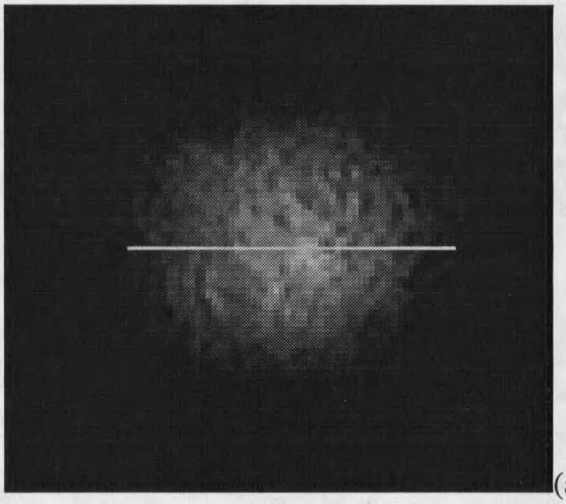
(a)

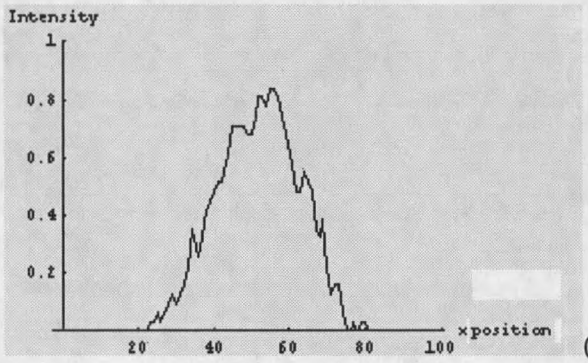

(b)

Figure 19: (a) The photon echo

(b) The intensity profile along the yellow line in part a

The third beam and its intensity profile are shown in figure 20. Obtained by inserting SH1 or SH2 in figure 15, which prevents the formation of the two pulse echo by only allowing one pulse through the medium. Again, the line indicates the position of the intensity profile in the same arbitrary units as figure 19.

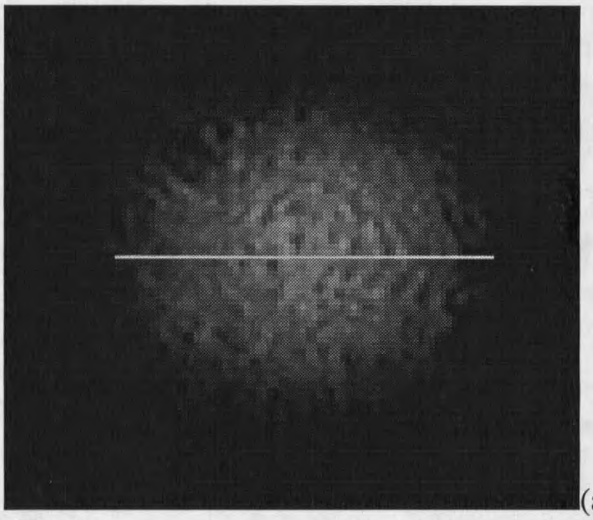

(a)

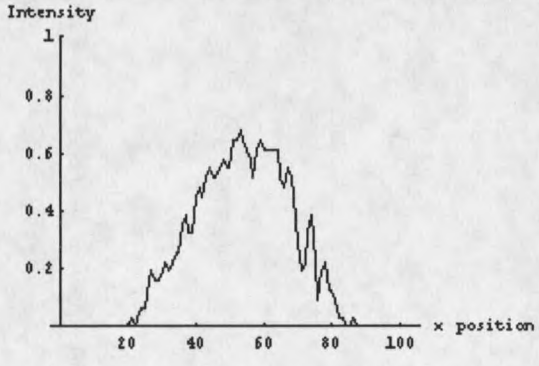

(b)

Figure 20: (a)The third beam

(b) An intensity profile from part a

In order to construct the correct type of logic gate, we are seeking destructive interference between the echo and the third input pulse. The delay of the third pulse was adjusted with this goal in mind. Constructive interference will produce a system whose

truth table is not a Taffoli gate, and therefore not universal for reversible computations. The lower the signal observed by the detector in the direction of the third pulse, the better the contrast between the two binary values that will be used in the truth table in figure 23. Naturally, we seek the greatest contrast possible to insure the detector will return the correct value when required.

The interference was observed by the camera in channel three, after allowing all three pulses to propagate through the material. Figures 21 and 22 show two spatial interference patterns in the direction of the third beam captured at slightly different beam alignment conditions. The first of these, figure 21, shows an interference fringe passing through the image from the upper right curving down to the lower left. There is some structure in the center, which did not show up on either of the two pulses alone. This perhaps shows where the phase of the pulses was corrupted by the optics, such as a speck of dust on a mirror. The intensity appears to drop essentially to zero and clearly indicates that some type of destructive effect is canceling the field at this point.

Figure 22 displays another case where destructive interference occurred. The delay line of the third pulse has been adjusted slightly as has the angle of the third pulse. The interference fringe indicates that the echo and third pulse are not aligned precisely in the vertical direction. The three intensity profiles are meant to show that the intensity of the light beam emerging in the third beam direction indeed does decrease in the destructive region.

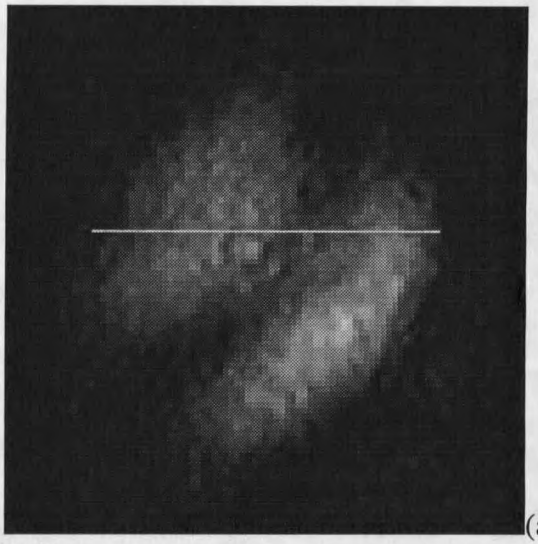

(a)

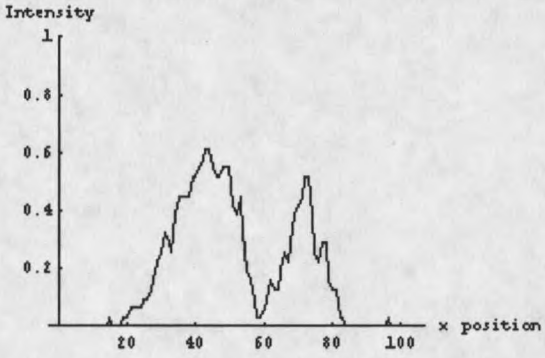

(b)

Figure 21: (a) Destructive interference

(b) Intensity profile of part a

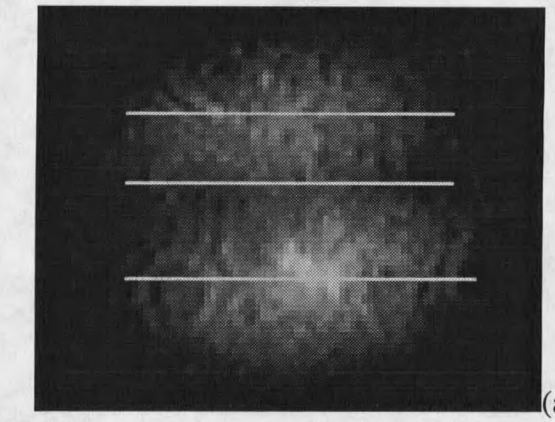

(a)

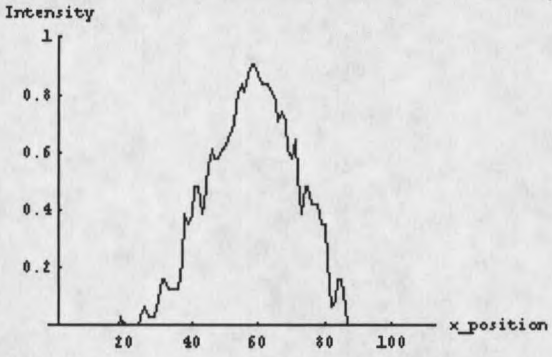

(b)

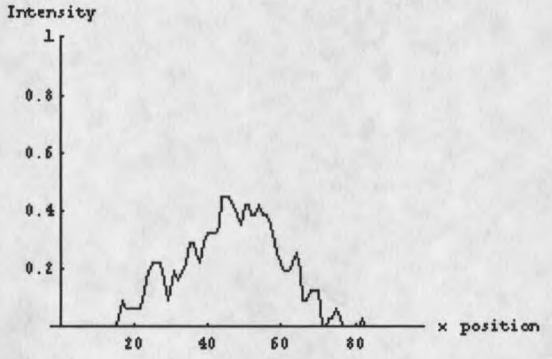

(c)

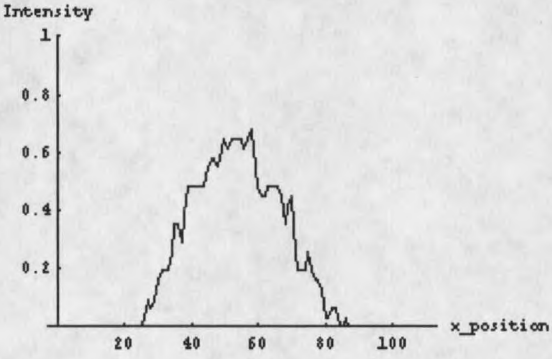

(d)

Figure 22: (a) Destructive interference (b) Intensity profile from upper line in part a (c) Intensity profile from middle line in part a (d) Intensity profile from lower line in part a

The essential causal nature of the photon echo generation process insures that an echo generated between the third pulse and the second pulse will not appear in any of the three directions. If such an echo was present, then it would alter the structure of the logical gate. Such an event could only occur with the second pulse leading the third pulse and an echo produced at a total angle of 4θ, out of the range of the output cameras. If the converse were allowed to take place, violating causality, then an echo would also be produced in the same path as the first pulse. Non-causal echo signals would disrupt the truth table formed from this system, and invalidate its function as a universal gate for quantum operations. We also note that a simple self-diffraction process of three beams intersecting in a light sensitive medium will give unwanted diffraction signals, which are not present in the photon echo arrangement.

We will also point out that this is an ultrafast gate. The pulses are hundreds of femtoseconds in duration, separated by 13.6 ns. Each excitation pulse pair will produce an echo, which may or may not interfere with a third pulse. So this gate, as described here, could perform logical operations at 76 MHz, the repetition rate of the laser pulses.

Let us now discuss the operation of the gate in more detail. If we put a detector in the path of the first, second, and third/echo pulses and consider the first second and third pulses as inputs, we can construct a truth table, figure 23. If the input beam is blocked and not allowed to pass through the SHB material, it is represented as a zero. If the pulse is allowed to pass through the material, it is represented as a one. On the output end, if the detector measures a signal, it appears in the truth table as a one, and if there is no signal, it is a zero.

the detector measures a signal, it appears in the truth table as a one, and if there is no signal, it is a zero.

Causal Gate

Input Channels			Output Channels		
beam 1	beam 2	beam 3	beam 1	beam 2	beam 3
0	0	0	0	0	0
0	0	1	0	0	1
0	1	0	0	1	0
0	1	1	0	1	1
1	0	0	1	0	0
1	0	1	1	0	1
1	1	0	1	1	1
1	1	1	1	1	0

Non-Causal Gate

Input Channels			Output Channels		
beam 1	beam 2	beam 3	beam 1	beam 2	beam 3
0	0	0	0	0	0
0	0	1	0	0	1
0	1	0	0	1	0
0	1	1	1	1	1
1	0	0	1	0	0
1	0	1	1	0	1
1	1	0	1	1	1
1	1	1	1	1	0

Figure 23: Taffoli Gate

In figure 23, you can see the result of blocking the input beams with the shutters in figure 15. The first line corresponds to all three shutters SH1, SH2, and SH3 closed. What is observed at the output is zero signal in all three channels. In the second line, SH1 and SH2 are both closed, but the third beam is allowed into the system by opening SH3. The first six lines progress in this way, with a 1 representing an open shutter on that channel, and a 0 stands for a closed shutter. The output channels all correspond exactly to the input channels for these six lines. We concentrate our attention on lines seven and eight, where the behavior is not trivial. The first two pulses are both allowed into the system. This event generates a photon echo in the same direction as the third

then what is observed is only the photon echo, and the detector registers a 1. Meanwhile, if SH3 is open, the two signals interfere, and although the input bit is a 1, the third output channel detector registers a 0.

The second gate shown in figure 23, is an example of what the truth table would look like if non-causal solutions were allowed. The problem occurs in the fourth line. Consider that pulse three had back reacted with pulse two, violating causality, and generated an echo pulse in the direction of channel 1. This would cause a 1 to register in the output, while a 0 was input to this channel, clearly altering the truth table logic structure.

The corresponding logic element is called a Taffoli Gate [5]. It functions as a controlled, controlled NOT. If there is a one input value in channel three, the output of channel three is a zero, and vise-versa. Where the first and second channels act as controllers and the "not" operation on the third bit only occurs if both have the value 1. The not process occurs if both input pulses are allowed to pass through the medium. They generate a photon echo, and if the third pulse is allowed into the system, the two destructively interfere and the output bit in channel three is a zero. If the third pulse is not allowed to pass through the medium, the third input bit is zero, and only the echo signal appears at the detector. The third output bit is then 1, not 0. The corresponding truth table is given by figure 23.

Let us consider now an expanded version of the version of the logic gate with four inputs and four outputs. If there is sufficient conversion efficiency in the echo process, more bits, input and output, may be added. Additional input pulses could interfere with higher order echoes. Figure 24 gives a possible geometry for such a system. Sufficient

efficiency would allow for the next order photon echo to be observed at yet another angle θ relative to the first order echo. This makes this signal at a total angle of 3θ from the first pulse. In the same way as with the first order echo, a fourth pulse can be directed in the direction of this second echo, delayed by the appropriate phase to produce destructive interference. You could continue to add channels until the highest order echo signal is on the order of the resolution of the interference effects. Gates of this type should also be reversible, and therefore universal for quantum computations. However, the additional bits allow larger "words" to be used in the operation, and the benefits of parallel processing come to mind.

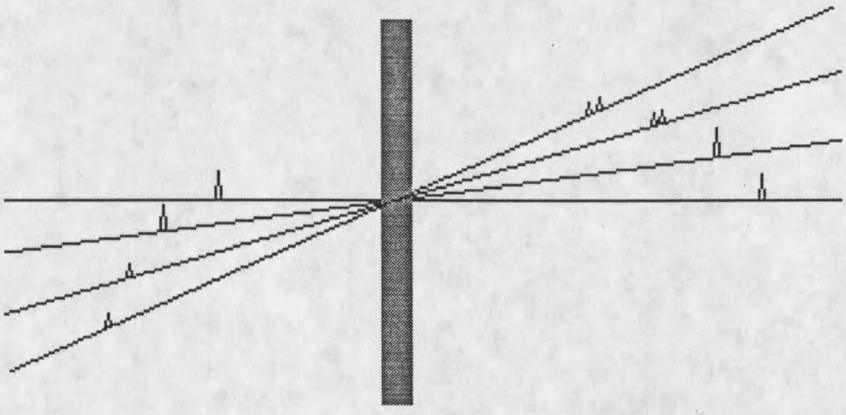

Figure 24: Interference with higher order echoes

The causality condition is even more important in this case. As the number of inputs goes up, the number of interactions between also increases, and the number of possible non-causal echoes, also increases. One must be very careful when constructing truth tables for gates with additional inputs. The truth tables for casual and non-causal four input gates of this type are given by figure 25. When considering the four

input/output truth table, keep in mind that only pulses arriving in the proper order will produce echoes. For example, pulse 1 followed by pulse 2 can create an echo in the direction of 3, and even pulse 2 and pulse 3 can produce an echo in the direction of 4. But pulse 3 and pulse 2 will not produce an echo in the direction of 1. The non-causal truth table illustrates how this, and similar non-causal events, would alter the logic structure. Lines 9 and 10 in the non-causal table are the very case described above, pulses 3 and 2 generate an echo in the direction of 1. Line 12 is an example of pulse 4 and 3 creating an echo in the direction of 2.